Role of a Conserved Glutamine Residue in Tuning the Catalytic Activity of *Escherichia coli* Cytochrome *c* Nitrite Reductase[†]

Thomas A. Clarke,[‡] Gemma L. Kemp,[§] Jessica H. Van Wonderen,[§] Rose-Marie A. S. Doyle,[§] Jeffrey A. Cole,[||] Nick Tovell,[||] Myles R. Cheesman,[§] Julea N. Butt,[§] David J. Richardson,*[,‡] and Andrew M. Hemmings*[,‡,§]

Centre for Molecular and Structural Biochemistry, School of Biological Sciences and School of Chemical Sciences and Pharmacy, University of East Anglia, Norwich NR4 7TJ, United Kingdom, and School of Biosciences, University of Birmingham, Edgbaston, Birmingham B15 2TT, United Kingdom

Received October 30, 2007; Revised Manuscript Received January 9, 2008

ABSTRACT: The pentaheme cytochrome *c* nitrite reductase (NrfA) of *Escherichia coli* is responsible for nitrite reduction during anaerobic respiration when nitrate is scarce. The NrfA active site consists of a hexacoordinate high-spin heme with a lysine ligand on the proximal side and water/hydroxide or substrate on the distal side. There are four further highly conserved active site residues including a glutamine (Q263) positioned 8 Å from the heme iron for which the side chain, unusually, coordinates a conserved, essential calcium ion. Mutation of this glutamine to the more usual calcium ligand, glutamate, results in an increase in the K_m for nitrite by around 10-fold, while V_{max} is unaltered. Protein film voltammetry showed that lower potentials were required to detect activity from NrfA Q263E when compared with native enzyme, consistent with the introduction of a negative charge into the vicinity of the active site heme. EPR and MCD spectroscopic studies revealed the high spin state of the active site to be preserved, indicating that a water/hydroxide molecule is still coordinated to the heme in the resting state of the enzyme. Comparison of the X-ray crystal structures of the as-prepared, oxidized native and mutant enzymes showed an increased bond distance between the active site heme Fe(III) iron and the distal ligand in the latter as well as changes to the structure and mobility of the active site water molecule network. These results suggest that an important function of the unusual Q263-calcium ion pair is to increase substrate affinity through its role in supporting a network of hydrogen bonded water molecules stabilizing the active site heme distal ligand.

A broad range of enteric bacteria express a cytochrome *c* nitrite reductase (NrfA[1]) that is synthesized under anaerobic conditions in the presence of low nitrate concentrations and a carbon source such as glycerol (*1, 2*). This periplasmic enzyme catalyzes the 6 e^- reduction of nitrite to ammonia. It can also convert the potential intermediates of nitrite reduction, nitric oxide (NO) and hydroxylamine (NH_2OH), to ammonia and has been proposed to have a role in enteric NO detoxification (*3*).

In γ-proteobacteria such as *Escherichia coli*, the *nrf* operon encodes membrane proteins NrfD and NrfC together with a periplasmic soluble protein NrfB to act as a transient electron donor chain to the terminal reductase, NrfA. In ϵ-proteobacteria such as *Wolinella succinogenes* and *Sulfurospirillum deleyianum*, and in δ-proteobacteria such as *Desulfovibrio desulfuricans*, however, the reductase exists as a stable NrfA:NrfH complex (*2, 4*). Crystal structures of representative electron donors of both types revealed significant structural differences between the tightly bound electron donor, NrfH (*5*), and the transient electron donor, NrfB (*6, 7*).

Although the method of electron input to NrfA differs between the two bacterial systems, the active site is highly conserved. The X-ray crystal structures of NrfA from *E. coli* (*8*), *W. succinogenes* (*9*), *S. deleyianum* (*10*), *D. desulfuricans* (*11*) and the NrfHA complex from *Desulfovibrio vulgaris* (*5*) have been solved and show NrfA to be a homodimeric enzyme with each monomer containing two calcium ions and five covalently attached *c*-type hemes that are named hemes 1 to 5 according to their position in the amino acid sequence. Four hemes are attached by conventional CXXCH sequence motifs and have bis-histidine ligands, while the fifth active site heme (heme 1) is attached through a unique CXXCK motif that provides a lysine residue to the proximal side of the heme. The distal ligand is provided by a water/hydroxide that is displaced in the presence of substrates such as nitrite. In addition to the lysine ligand, Lys 126 (all residue numbering refers to the *E. coli* NrfA), there are four further

[†] This work was supported by BBSRC grants B18695 to D.J.R., A.M.H., J.N.B., M.R.C., and J.A.C. and Wellcome Trust JIF grant 0162178 to D.J.R., A.M.H., J.N.B., and M.R.C.

* To whom correspondence should be addressed. David Richardson or Andrew Hemmings, School of Biological Sciences, University of East Anglia, Norwich NR4 7TJ, U.K. Tel: +44(0)1603-592269. Fax: +44(0)1603-592250. E-mail: d.richardson@uea.ac.uk (D.J.R.); a.hemmings@uea.ac.uk (A.M.H.).

[‡] School of Biological Sciences, University of East Anglia.

[§] School of Chemical Sciences and Pharmacy, University of East Anglia.

[||] University of Birmingham.

[1] Abbreviations: NrfA, cytochrome *c* nitrite reductase; e^-, electron; rmsd, root-mean-square deviation; EPR, Electron Paramagnetic Resonance; MCD, Magnetic Circular Dichroism; PFV, Protein Film Voltammetry; i_{cat}, experimentally determined catalytic current; $E_{cat,}$ the potential at the steepest part of the catalytic wave associated with the onset of catalysis.

10.1021/bi702175w CCC: $40.75
Published on Web 03/01/2008

conserved active site residues, Tyr 216, Arg 106, Gln 263, and His 264, that are proposed to contribute to a electropositive environment within the active site pocket that allows access to the negatively charged substrate, nitrite (NO_2^-). Some of these residues are also believed to act as proton donors during enzyme turnover (*12*). The active site QH dipeptide sequence motif comprising Gln 263 and His 264 is highly conserved in NrfA sequences, and in Ramachandran plots, His 264 is the only residue to fall in the generously allowed regions, suggesting an important structural or catalytic role for this residue.

In all available crystal structures of NrfA enzymes (*5, 8–11*), an octahedrally coordinated calcium atom (calcium I) is present ~11 Å from the active site heme iron. This calcium ion appears to play a role in maintaining active site structure, most notably by preventing His 264 from occupying the distal coordination site of heme 1 (*11*) and in contributing positive charge to the surface of the substrate access channel (*10*). The coordination sphere of this ion comprises both oxygen atoms of the carboxyl group of Glu 215, the main chain carbonyl groups of Lys 261 and Tyr 216 as well as two water molecules. The final ligand to this calcium ion is the side chain amide oxygen atom of Gln 263. Analysis of the 3368 calcium-containing structures in the Protein Data Bank reveals that while aspartate, glutamate and asparagine contribute a total of 67% of the 36175 calcium ion ligands, glutamine is responsible for only 3.2%. In fact, where glutamine provides a calcium ligand, the glutamine side chain amide oxygen atom comprises only 1.6% of the total calcium ligand interactions. In the 269 structures where these ligands occur, the majority are at the surface of the protein and, in the case of enzymes, away from the active site. The NrfA enzymes represent the only family where this conserved glutamine−calcium ion pair is close enough to the active site to be involved in enzyme activity. Hence, the adoption of glutamine for this role in the active site of NrfA may be important to function. Calcium ions positioned close to the active sites of enzymes often fulfill functional roles. For example, in horseradish peroxidase calcium ions are present on both the proximal and distal sides of the active site heme, where they play a role in stabilizing the structure of the functional enzyme (*13*). The structural similarities between the location of the calcium sites on the distal side of the catalytic hemes in NrfA and in class II and III peroxidases has previously led to the suggestion that they may share similar physiological roles (*11*).

To help provide insights into the roles that the active site calcium ion and coordinating glutamine residue may have in nitrite reduction to ammonia by cytochrome *c* nitrite reductase, we have mutated the glutamine at position 263 in *E. coli* NrfA to the more usual calcium ligand, glutamate. The changes that occur to the structure and activity of the enzyme revealed by a combination of X-ray crystallography, electron paramagnetic resonance (EPR), magnetic circular dichroism (MCD), enzyme kinetics and protein film voltammetry (PFV) show that this residue modulates the operating potential of the enzyme and also increases affinity for the substrate nitrite by anchoring a network of water molecules at the active site.

MATERIALS AND METHODS

Mutation and Expression of NrfA Q263. The template used to introduce the Q263E substitution in *nrfA* was plasmid pJG1.2, which is a derivative of pJG1 (*14*) from which the 4 kb fragment from the *Hin*dIII site in *nrfC* to the *Eco*RI site downstream of *nrfG* had been deleted. Plasmid pJG1.2, therefore, encodes only NrfA and NrfB. The Q263E substitution was introduced into the *nrfA* gene on plasmid pJG1 using the Quikchange Site-Directed Mutagenesis kit (Stratagene) following the manufacturer's instructions. The forward primer was JR Q263E FOR, 5′ CGCCAATGCTGAAAGCG**GAA**CACCCGGAATATGAAACC 3′; the reverse primer was JR Q263 REV, 5′ GGTTTCATATTCCGGGT**GTTC**CGCTTTCAGCATTGGCG 3′ (the three bases of codon 263 are underlined; bases in bold text show changes from the original sequence). Plasmids isolated from transformants after mutagenesis were confirmed by sequencing the complete coding region of the *nrfA* gene. No unexpected substitutions were found.

Plasmid pJG1.9aQ263E was transformed into the *E. coli* strain JCB4083a cells that have the genotype Δ*narZ::ω*Δ *narL::Tn10*Δ*napGH*Δ*nrfAB*Δ*nirBDC*::Kan^R and also contained the cytochrome *c* maturation plasmid pEC86 (*15*). Transformed cells were grown aerobically overnight at 37 °C in 10 L of Terrific Broth with 100 μg/mL carbenicillin and 30 μg/mL chloramphenicol. Approximately 150 g of cells were harvested by centrifugation and stored at −80 °C until required.

Purification of NrfA Variants. Both native NrfA and NrfA Q263E were purified according to published procedures (*16*). Briefly, cells were resuspended in 1 L of sphaeroplastic buffer (100 mM Tris, pH 7.0, 1 mM EDTA, and 500 mM sucrose) and incubated for 30 min with lysozyme at a final concentration of 1 mg/mL. The incubated cells were centrifuged for 1 h at 9,000*g*, and the NrfA containing supernatant was decanted.

Ammonium sulfate was added to the supernatant to a final saturation of 65% and left stirring for 3 h at 4 °C to precipitate NrfA. The supernatant was centrifuged at 30,000*g*, and the pellet containing precipitated NrfA was resuspended in 100 mL of 50 mM Tris at pH 8.0. This resuspended NrfA was then dialyzed against 5 L 50 mM Tris at pH 8.0 to remove excess ammonium sulfate. Dialysis was repeated three times to ensure that excess salt was removed.

The dialysed solution containing NrfA was loaded onto a 25 × 2.5 cm Q-sepharose column (Amersham Biosciences) equilibrated with 50 mM Tris at pH 8.0 and washed with 100 mL of 50 mM Tris at pH 7.0. Protein was eluted using a gradient of 0–200 mM NaCl in 50 mM Tris at pH 8.0 over 150 mL. Five milliliter fractions were collected, and the presence of NrfA was determined using SDS−polyacrylamide gels stained for the presence of heme (*3*). Fractions containing NrfA were pooled and concentrated before passage through a Superdex 200 26/60 gel filtration column (Amersham Biosciences) pre-equilibrated with 50 mM Tris at pH 7.05 and 100 mM NaCl. Fractions containing NrfA were identified using Coomassie stained SDS−polyacrylamide gels and dialyzed against 50 mM Tris at pH 7.0.

As a final purification step, dialyzed fractions containg NrfA were loaded onto a Mono-Q 5/50 column (Amersham Biosciences) equilibrated with 50 mM Tris at pH 7.0 and

eluted using a gradient of 0–200 mM NaCl and 50 mM Tris at pH 7.0. Fractions were checked for purity using Coomassie stained SDS−polyacrylamide gels. NrfA fractions that eluted as a single band were pooled and concentrated to 10 mg mL^{-1}. The yield of purified NrfA Q263E was 0.5 mg from 10 L of culture.

Methyl Viologen Assays. The rate of methyl viologen oxidation was used to measure the rate of electron input to NrfA as described previously (*16*). Electrons transferred to NrfA from methyl viologen previously reduced with sodium dithionite caused a change in the absorbance of methyl viologen that could be measured at 600 nm. A molar extinction coefficient of 13.7 mM^{-1} cm^{-1} was used to convert the change in absorbance to the number of electrons transferred to the enzyme.

The amount of ammonium formed during the turnover of both enzymes was measured according to published procedures (*17*). An incubation mixture containing 50 mM HEPES at pH 7.0, 2 mM $CaCl_2$, 5 mM $NaNO_2$, 1 mM methyl viologen and 3 nM NrfA was sparged with N_2 and incubated at 25 °C before the addition of 2 mM $Na_2S_2O_4$ to start the reaction. After 5 min, the reaction was stopped by vortexing the assay mixture in air to oxidize the excess reductant. The amount of ammonia formed was measured using the NADH dependent formation of glutamate from α-ketoglutarate and ammonia (*17*).

Protein Film Voltammetry of NrfA. Cyclic voltammetry was performed using a three-electrode cell configuration as described previously (*18, 19*). The reference electrode employed was Ag/AgCl (saturated KCl). All potentials are quoted versus the standard hydrogen electrode, achieved via the addition of 0.197 V to experimental data. The electrochemical cell was housed in a Faraday cage within a nitrogen-filled anaerobic chamber maintained at <5 ppm O_2. Immediately prior to each experiment, the pyrolytic graphite edge working electrode was polished with an aqueous slurry of 0.3 μm alumina, rinsed and dried with a tissue. Protein films were formed by placing 1 μL of ice-cold NrfA sample (0.15 μM NrfA Q263E or 0.17 μM native in 50 mM HEPES and 2 mM $CaCl_2$ at pH 7.0) directly onto the electrode surface for approximately 10 s, then removing the excess. The electrode was immediately placed into an electrochemical cell containing 50 mM HEPES and 2 mM $CaCl_2$ at pH 7.0 and 20 °C. Stock solutions of $NaNO_2$ were prepared fresh daily in ice-cold buffer and thoroughly purged with argon prior to their addition to the electrochemical cell. To quantify the catalytic activity, the current measured at −0.6 V in the absence of nitrite was subtracted from each voltammogram in the presence of nitrite to give the catalytic current. Signal loss was noted during the course of experiments and found to be a first order process. Prior to analysis, catalytic currents were corrected for this effect using rate constants of 1.7×10^{-4} s^{-1} for NrfA Q263E and 4×10^{-4} s^{-1} for native NrfA. Data were fitted to the Michaelis–Menten equation using Origin (Microcal Software Inc.).

EPR and MCD Spectroscopies. EPR spectra were measured with a Bruker ER300D spectrometer fitted with a dual mode cavity type ER4116DM interfaced to an ELEXSYS computer control system (Bruker Analytische Messtechnik GmBH) and equipped with a variable temperature cryostat and liquid helium transfer line (Oxford Instruments). MCD spectra were recorded on JASCO circular dichrographs models J810 and J730 for the UV–visible and near-infrared (NIR) regions, respectively, used in conjunction with an Oxford Instruments superconducting solenoid 6 T SM1 magnet with an ambient temperature sample bore. The intensities of spectra presented are referred to concentrations based on an extinction coefficient of 497,650 $M^{-1}cm^{-1}$for the Soret absorption bands near 409 nm. Samples were prepared in deuterium oxide solutions containing 50 mM HEPES and 2 mM $CaCl_2$. pH* is the apparent pH of the D_2O-based solutions measured using a standard glass pH electrode.

Crystallization and X-ray Data Collection. Native NrfA was crystallized under conditions different from those described previously (*8*). Briefly, purified enzyme was concentrated to 10 mg ml^{-1} and centrifuged at 16,000*g* for 10 min at 4 °C before crystallization. Crystals were obtained under aerobic conditions by the vapor diffusion hanging drop method using 20% (v/v) PEG 10K in 100 mM Na-HEPES at pH 7.5. For data collection, single crystals were soaked with a solution of reservoir buffer containing 20% (v/v) ethylene glycol as a cryoprotectant. X-ray diffraction from single crystals was measured using an ADSC detector on beamline ID-29 at the ESRF (Grenoble). The native NrfA crystal chosen for data collection was of space group $P2_1$ with cell dimensions $a = 90.4$ Å, $b = 79.3$ Å, $c = 137.6$ Å, $\alpha = \beta = 90°$, and $\gamma = 101.5°$. These cell dimensions are highly similar to those reported previously in the determination of the structure of the native *E. coli* enzyme at 2.5 Å resolution (*8*). The recombinant NrfA Q263E crystals were of space group $P2_12_12_1$ with cell dimensions $a = 82.3$ Å, $b = 91.2$ Å, $c = 295.5$ Å, and $\alpha = \beta = \gamma = 90$ °. In both crystal forms, the solvent content was approximately 45% (v/v) with four molecules of NrfA in the crystallographic asymmetric unit. Diffraction data sets for both native NrfA and NrfA Q263E were obtained from single crystals to resolutions of 1.74 Å and 2.04 Å, respectively, using X-ray wavelengths of 0.931 and 0.992 Å. Data sets were processed using MOSFLM (*20*) and SCALA (*21*) as part of the CCP4 package (*22*). Data collection statistics are summarized in Table 1.

In attempts to solve crystal structures for the nitrite adducts of NrfA and NrfA Q263E, single crystals of both enzymes were soaked for 5 min at 4 °C in solutions of mother liquor supplemented with varying concentrations of nitrite up to 100 mM before transfer to similar solutions to which 20% (v/v) ethylene glycol had been added. X-ray diffraction data sets were then collected and processed using representative crystals in the same manner as that described above for the free oxidized enzymes.

Crystal Structure Solution and Refinement. A high resolution structure of oxidized native NrfA at 1.74 Å resolution was determined by molecular replacement using a single monomer from the 2.5 Å resolution structure of the native enzyme available in the Protein Data **b**ank (PDB entry 1GU6) (*8*) as a search model. Molecular replacement using MOLREP as part of the CCP4 package (*22*) was used to generate an initial structural model that contained four NrfA monomers in the asymmetric unit. This model was improved by alternating rounds of manual model building using COOT (*23*) and automatic refinement using REFMAC (*24*). Addition of 2149 water molecules using ARP (*25*), four sulfate ions and 32 ethylene glycol molecules gave a final structure

Table 1: X-ray Data Collection and Refinement Statistics

	NrfA native	NrfA Q263E
data collection[a]		
wavelength (Å)	0.931 Å	0.992 Å
resolution (Å)	31.3 − 1.74 (1.82 –1.74)	79 − 2.04 (2.15 − 2.04)
unique reflections	193,651 (26,427)	137,863 (19,032)
completeness (%)	99.0 (92.9)	97.1 (92.9)
R_{sym} (%)	7.3 (35.1)	9.6 (32.7)
I/σ	7.7 (2.1)	3.6 (0.9)
multiplicity	3.9 (3.1)	3.7 (3.6)
average atomic B-factor (Å^2)	16.3	18.8
refinement[a,b]		
R_{cryst}	15.4 (28.0)	17.1 (21.8)
R_{free}	18.8 (34.5)	22.6 (26.3)
model		
protein atoms[c]	14026	13986
water	2149	1782
heme atoms	860	860
other	140	68
bond length rmsd (Å)	0.013	0.018
bond angle rmsd (°)	1.3	1.5
average atomic B-factor (Å^2)	16.8	22.0

[a] The values in parentheses indicate the highest resolution shell. [b] $R = \Sigma| F_o - F_c |/\Sigma F_o$. R_{cryst} is calculated with 95% of the data used during refinement. R_{free} is calculated with a 5% subset of data not used during refinement. [c] The difference in protein atoms is due to an increased number of dual conformations observable at increased resolutions. Both structures contain the same number of amino acids.

with R_{cryst} (R_{free}) of 15.4% (18.8%) for all data in the resolution range 31.3−1.74 Å. When analyzed for stereochemical quality using PROCHECK (*26*), the structure has 99.7% of residues in favored regions of the Ramachandran plot. The sole outlier is the active site residue His 264, which falls in the generously allowed region as previously reported (*8*). No residues fall in disallowed regions.

The structure of NrfA Q263E was determined by molecular replacement using as a search model the refined 1.74 Å resolution native NrfA structure from which sulfate ions, water and cryoprotectant molecules had been removed. This was corrected by cycles of manual model building and automatic refinement in the same fashion as that used for the structure of the native protein. After the addition of 1782 water molecules and 15 ethylene glycol molecules, the refined structure had an R_{cryst} (R_{free}) of 17.1% (22.6%) for data in the resolution range 79.0 – 2.04 Å. Stereochemical quality analysis using PROCHECK revealed the structure has the same Ramachandran distribution as the 1.74 Å native structure. Average rmsd values were calculated using SUPERPOSE as part of the CCP4 package (*22*) and use both main chain and side chain atoms.

The refined coordinates have been deposited to the Protein Data Bank with accession numbers 2RDZ and 2RF7 for the native and Q263E enzymes, respectively.

RESULTS

Spectroscopic Properties of Native and Mutant NrfA. NrfA Q263E was purified and observed to run as a single band on Coomassie-stained SDS−polyacrylamide gels. The room temperature MCD (RT-MCD) spectra of NrfA Q263E in the UV–visible and near-infrared (NIR) regions are shown in Figure 1A and B, respectively. Figure 1C and D show analogous spectra for the native enzyme as previously reported (*8*). The salient points in the MCD spectra of native and mutant protein are the same. The Soret region (350–450 nm) is dominated by a derivative-shaped feature characteristic of low-spin ferric heme (*27*). The intensity of this feature is

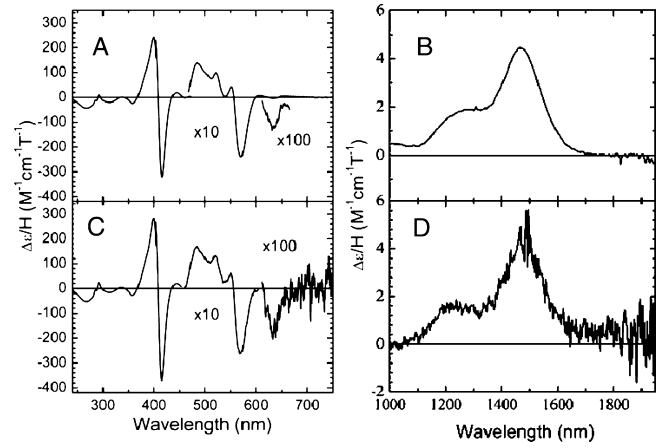

FIGURE 1: Room temperature MCD spectra comparing the native NrfA and NrfA Q263E. (A) UV–visible region and (B) NIR region of native NrfA; (C) UV–visible region and (D) NIR region of NrfA Q263E. Samples were in 50 mM HEPES and 2 mM $CaCl_2$ at pH* 7.0. Spectra were recorded at room temperature and at a magnetic field of 6 T.

indicative of the presence of four such hemes. In the NIR region, the proteins give rise to a Fe^{III}(d)-to-porphyrin(π) charge-transfer (CT) band characteristic of low-spin ferric hemes. The exact position of this band is diagnostic of axial heme ligation (*28, 29*) and here is typical for hemes with two histidine ligands. Again, the intensity is consistent with the presence of four hemes. Generally, the weaker MCD bands of high-spin ferric hemes are only detectable, against the intense background of low-spin centers, in the region 600–750 nm. At these wavelengths, high-spin heme gives rise to a derivative-shaped CT band, the position of which is also indicative of axial ligation. This band is seen as a trough in Figure 1A and C. The positive part of the feature, to shorter wavelength, is obscured by the intense α-band of the four low-spin hemes. The band is relatively broad and spans the wavelengths found for hemes with a nitrogenous proximal ligand and water or hydroxide ion on the distal

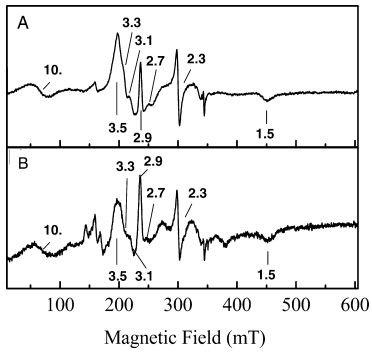

FIGURE 2: X-band EPR spectra comparing (A) native NrfA and (B) NrfA Q263E. Samples were in 50 mM HEPES and 2 mM $CaCl_2$ at pH 7.0. Spectrometer parameters: microwave power 2 mW; modulation 10 mT; temperature, 10 K. *g*-values are shown.

side. The mutant appears then to retain the mixed ligation observed at the active-site heme of the native enzyme (*8*).

The main features in X-band perpendicular-mode EPR spectra (Figure 2) are also unchanged for the mutant protein. A simple rhombic trio, with *g*-values of 2.9, 2.3, and 1.5, arises from bis-histidine coordinated heme in which the ligand planes are oriented parallel and are observed in both. Features at 3.1 and 2.7, which may arise from other low-spin hemes, also persist. The broad features at $g = 10$ and in the $g = 3.3$ region arise from a weak (J $\sim$1 cm^{-1}) coupling between $S = 1/2$ and $S = 5/2$ centers (*30*) and are due to an interaction between the high-spin active-site heme and one of the near-by low-spin centers. Such signals are extremely sensitive to small changes in *J*, and the similarity of the two EPR spectra in this respect indicates that the mutation has resulted in no structural changes at or near these two hemes.

Catalytic Properties of Native and Mutant NrfA. The catalytic properties of NrfA Q263E were assessed in solution using methyl viologen, reduced with sodium dithionite, as an electron donor (*8*) and by cyclic voltammetry with the enzyme adsorbed on graphite electrodes (*19*). Methyl viologen transfers electrons to NrfA through hemes exposed at the enzyme surface. Electrons are then transported through a chain of hemes to the active site, where they are used to reduce nitrite directly through the lysine-coordinated heme 1. Figure 3 shows the rate of nitrite reduction catalyzed by NrfA in the presence of increasing amounts of nitrite for both the native and mutant NrfA enzymes. The activity of the native NrfA is significantly higher at 50 μM nitrite when compared with NrfA Q263E, while the activity of both enzymes is similar at concentrations greater than 1 mM. The data were fitted using a Hanes plot to determine K_m and V_{max} values for the rate of nitrite reduction by both forms of NrfA. The K_m of the native NrfA was 33 $\pm$ 15 μM, and the V_{max} was 629 $\pm$ 25 NO_2^- s^{-1} at 25 °C, similar to the values previously determined (*8*). The K_m of NrfA Q263E was 413 $\pm$ 63 μM, more than 10-fold greater than the native NrfA K_m, while the V_{max} was 641 $\pm$ 41 NO_2^- s^{-1}, similar to the native NrfA and indicating that Gln 263 has a role in nitrite recognition but not in nitrite reduction.

The rate of ammonium formation at 5 mM NO_2^- by NrfA Q263E was measured as 533 $\pm$ 42 NH_4^+ s^{-1}, while the rate of methyl viologen oxidation under identical conditions was 3126 $\pm$ 144 e^- s^{-1}. The ratio of the electrons consumed to ammonia produced is 5.9 $\pm$ 0.7, indicating that NrfA Q263E,

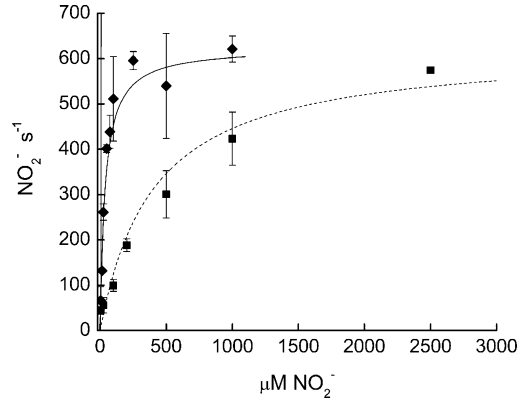

FIGURE 3: Comparison of nitrite reduction rates from native NrfA (♦) and NrfA Q263E (■) as measured by methyl viologen assays. Lines show Michaelis–Menten behavior with K_m values of 33 $\pm$ 15 μM and 413 $\pm$ 63 μM, and V_{max} values of 629 $\pm$ 25 and 641 $\pm$ 41 NO_2^- reduced s^{-1} for native NrfA and NrfA Q263E, respectively. Values are presented $\pm$ standard error. Experiments performed in 50 mM HEPES at pH 7.0 and 2 mM $CaCl_2$.

like the native enzyme (*31*), reduces nitrite stoichiometrically to ammonia.

Protein film voltammetry (PFV) of NrfA has been well characterized and provides a sensitive probe of catalytic properties of the enzyme (*18, 19, 32*). Previous titration of the native enzyme with nitrite yielded a K_m of around 25 μM, comparable to that found in methyl viologen activity assays (*8, 19*). NrfA Q263E is also amenable to study by PFV, with a reductive (negative) catalytic current observed in the presence of nitrite (Figure 4A). The catalytic response is more clearly viewed after subtraction of the voltammogram in 0 μM nitrite, which also allows ready quantitation of catalytic current magnitudes (i_{cat}) (Figure 4B). After baseline subtraction, the catalytic currents of the forward and reverse scans overlay, and the signal was found to be rotation rate independent indicating a steady state response. Plotting i_{cat} at -0.6 V versus nitrite concentration enabled the calculation of a K_m of 290 $\pm$ 50 μM for NrfA Q263E (Figure 4C). This is a value 10-fold greater than that for the native enzyme determined by PFV, and the behavior is in good agreement with that displayed in methyl viologen assays.

Protein film voltammetry provides additional information to methyl viologen based assays since the enzyme activity is defined across the electrochemical potential domain. For native NrfA, the activity versus potential profile exhibits a peaked response at nitrite concentrations below the K_m (Figure 4D). The peak reflects an increase in activity as the electrode potential is lowered followed by an attenuation of the activity to approach a constant, nonzero value. The two parts of the response are highlighted in plots of the first derivative of catalytic current with respect to potential, where they appear as a positive and negative peaks, respectively (Figure 5A and B); as the nitrite concentration is increased and the catalytic rate approaches V_{max}, the attenuation becomes less apparent, and a boost in activity starts to appear over a similar potential range (Figure 4D). Eventually, the enzyme-limited, that is, maximal, catalytic response is achieved where the attenuation is no longer present, and the profile shows that the onset of catalysis is followed by an additional boost in activity as the potential is lowered. Again, this is clearly illustrated in the first derivative plot where two positive peaks are apparent (Figure 5C).

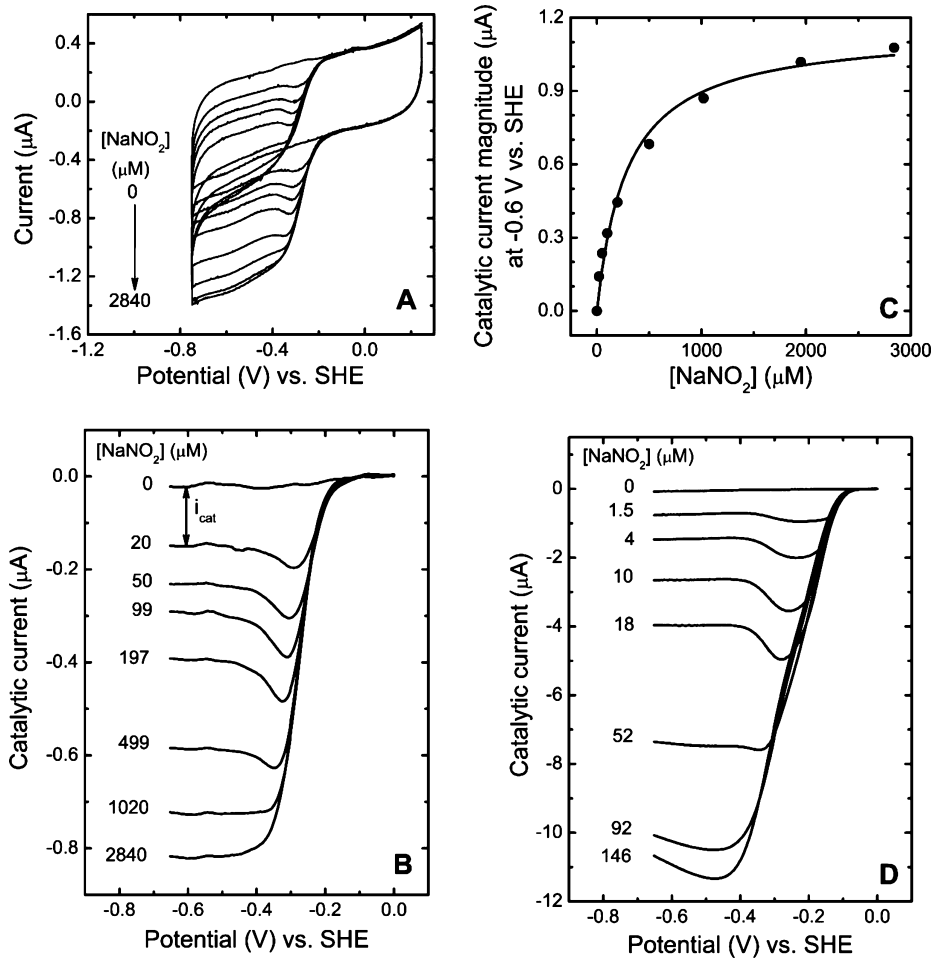

FIGURE 4: Protein film voltammetry of NrfA Q263E and native NrfA when titrated with nitrite. (A) Cyclic voltammograms of NrfA Q263E in nitrite concentrations of 0, 20, 50, 99, 197, 499, 1020, 1950, and 2840 μM. (B) Baseline-subtracted voltammetry of NrfA Q263E from panel A. Nitrite concentrations are as shown. Catalytic current magnitude (i_{cat}) at –0.6 V indicated for response at 20 μM nitrite. (C) Plot of catalytic current magnitude at –0.6 V versus nitrite concentration. Catalytic currents are presented after time correction of data in panel B. Line shows Michaelis–Menten behaviour with $K_m = 290$ μM and i_{max} (V_{max}) = 1.15 μA. (D) Baseline-subtracted voltammetric response of native NrfA in nitrite concentrations as shown. Experimental conditions are scan rate 30 mV/s, electrode rotation rate 3000 rpm, and buffer/electrolyte of 50 mM HEPES and 2 mM $CaCl_2$ at pH 7.0 and 20 °C.

For NrfA Q263E, when the nitrite concentration is less than the K_m, the catalytic profile is similar to that of native NrfA with a clear peak of activity (Figures 4B and 5A). However, as the nitrite concentration is raised and the catalytic rate approaches its maximal value, the waveshape deviates from that of the native enzyme. The attenuation is no longer visible, but no boost of activity is apparent as the wave describes an essentially sigmoidal increase in activity as the applied potential is lowered. Reflecting this waveshape, the current derivatives for NrfA Q263E at high nitrite concentrations show a single positive feature, in contrast to the two positive features displayed by native NrfA under equivalent conditions (Figure 5C).

Significantly, the overlaid first derivative plots also illustrate shifts in the potential dependence of the NrfA Q263E response relative to that of native NrfA (Figure 5). For NrfA Q263E, the nitrite reductase activity is turned on below ca. −150 mV, while less driving force is required to activate native enzyme with activity initiated below ca. −50 mV. The potentials of the peaks in the first derivative plots, E_{cat} for the positive feature at higher applied potential and E_{switch} for the negative feature, quantitate the positions of the corresponding features in the catalytic wave (Figure 5A). The negative displacement of NrfA Q263E activity compared to native enzyme is reflected in the relative values of E_{cat}, which are ca. 100 mV more negative for NrfA Q263E (−230 mV) than native NrfA (−130 mV). E_{switch} is also slightly more negative (ca. 35 mV) for NrfA Q263E when compared to the native enzyme.

High Resolution Crystal Structures of Native and Mutant NrfA. Native NrfA from *E. coli* crystallized in space group $P2_1$ with two dimers in the crystallographic asymmetric unit. The crystal structure was solved by molecular replacement and refined at high resolution (1.74 Å). The most significant difference between the structures of the two dimers in the asymmetric unit was a small rotation of monomers at the dimer interface; the *E. coli* NrfA dimer has a dissociation constant of 4 μM (*7*), which may reflect the flexibility of the dimer interface. The existing 2.5 Å resolution crystal structure of the enzyme (PDB entry 1GU6) was solved in space group $P2_12_12_1$ (*8*). Thus, small changes in the packing at the dimer interface allow purified *E. coli* NrfA to produce two different crystal forms from similar crystallization conditions. The average pairwise rmsd of the four NrfA monomers in the high resolution structure is only 0.63 Å, and the monomers are thus essentially identical. The arrangement of the five conserved active site residues is very similar to that found in the high resolution crystal structures

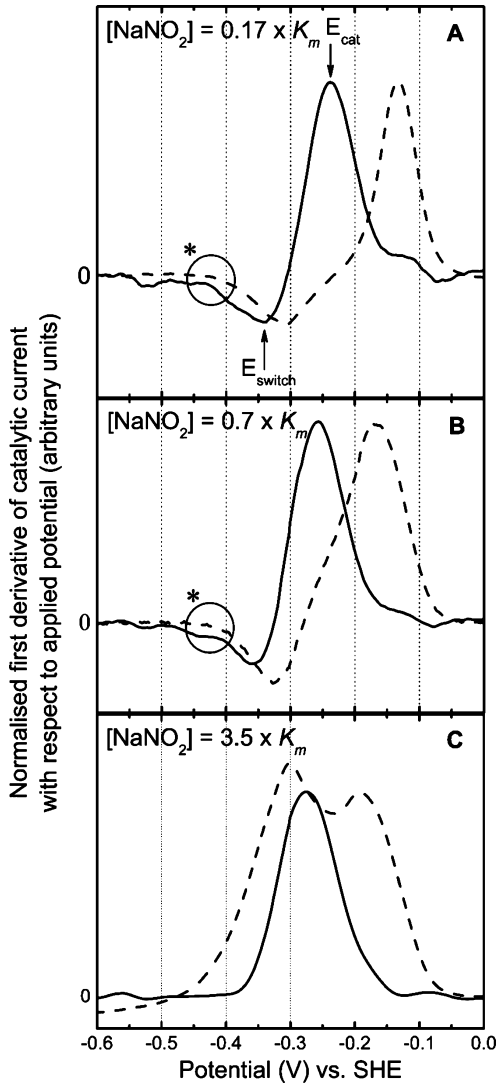

FIGURE 5: Comparison of the catalytic current–potential profiles of Q263E and native NrfA at nitrite concentrations below (A), near (B), and above (C) the K_m for nitrite. Profiles are shown as the first derivatives of catalytic current with respect to potential to emphasize their multiple features (see text for details). (—) NrfA Q263E and (---) native NrfA. Nitrite concentrations are as indicated where $K_m = 290\ \mu M$ for NrfA Q263E and $K_m = 25\ \mu M$ for native NrfA. In panel A, the features E_{cat}, E_{switch} and the region of the foot of the attenuation wave (*) are indicated for the Q263E derivative. Experimental conditions are as described in Figure 2.

of the *W. succinogenes* and *S. deleyianum* NrfA enzymes (solved at 1.6 Å and 1.9 Å resolution, respectively) differing by an rmsd of only 0.28 and 0.26 Å. However, the new high resolution structure of *E. coli* NrfA has allowed the definition of ordered water molecules in the active site. The positions of these active site water molecules are highly conserved across the four monomers in the asymmetric unit as well as in the structures from *W. succinogenes*, *S. deleyianum* and *D. desulfuricans*. The water network around the active site has been proposed to provide protons to the active site and allow product access and egress (*10*). Five of the conserved water molecules in the active site of NrfA are shown in Figure 6A. The first of these (labeled W1) is the distal water molecule bound to heme 1 and hydrogen bonded to the side chain of His264. Two further water molecules form direct hydrogen bonding interactions with W1: one water molecule bridging W1 and the phenolic hydroxyl group of Tyr 216

Table 2: Variation in the Coordination Distances of the Active Site Axial Heme Ligands and Overall Amino Acid B-Factor of the Polypeptide Chains in the Four Monomers of NrfA

NrfA	chain	distal ligand (Å)	proximal ligand (Å)	B-factor (Å^2)	contacts[a]
native	A	2.28	2.15	14.9	95
	B	2.17	2.19	13.4	100
	C	2.27	2.24	17.3	79
	D	2.32	2.18	13.4	123
	mean[b]	2.26 ± 0.03	2.26 ± 0.02		
Q263E	A	2.52	2.03	20.8	72
	B	2.49	2.40	18.0	71
	C	2.55	2.12	17.4	77
	D	2.77	2.00	28.1	59
	mean[b]	2.58 ± 0.06	2.14 ± 0.08		

[a] Contacts refer to the number of residues involved in interactions between neighboring polypeptide chains in the crystal lattice and were determined using MSD PISA (*37*) at the European Bioinformatics Institute (http://www.ebi.ac.uk/msd-srv/prot_int/pistart.html). [b] The values are presented ± standard error.

(W2) and the other coordinated by the carboxyls of the two propionate groups of heme 1 (W3). Two further conserved water molecules hydrogen bond to the side chains of active site residues. These are a water molecule (labeled W4) bridging the guanidinium group of Arg 106 and W2 and a final water hydrogen bonded to Tyr 216 and Gln 263 (labeled W5). The water distal ligand to the active-site iron has a coordination distance of 2.26 ± 0.03 Å (Figure 6A and Table 2). This is similar to the distance (2.17 ± 0.02 Å) observed in the previously determined 2.5 Å resolution structure of the *E.coli* enzyme (*8*) and only marginally longer than those observed in the structures of the *W. succinogenes* (2.03 Å) and *D. desulfuricans* enzymes (2.09 ± 0.01 Å).

In both the native and NrfA Q263E structures, the atomic temperature factors (B-factors) in the region around heme 2, including several α-helices at the surface of the molecule, are typically higher than other regions of the enzyme. This is most evident in the crystal structure of the NrfA Q263E enzyme where one chain has significantly higher B-factors in the region of heme 2 than the other three chains, suggesting that this region is more mobile than the corresponding regions in analogous domains. Polypeptide chains that have more extensive surface contacts in the crystal lattice have lower B-factors (Table 2). We attribute the variance in B-factor to the differences in interface and symmetry-related contacts between the monomers (Table 2) and propose that a decrease in surface contacts around the region of heme 2 allows this region more freedom. The area around heme 2 is the binding site of the electron donor NrfB (*7, 8*), and in the NrfHA structure, the electron donor causes significant movement of the chains around heme 2 (*5*). It is, therefore, likely that the high B-factors observed in these regions of the chain reflect an intrinsic flexibility that allows NrfA to adjust its structure locally to form a tight complex with NrfB.

The NrfA Q263E protein crystallized in space group $P2_12_12_1$ with cell dimensions similar to those found in the original 2.5 Å native structure (*8*). The structure of NrfA Q263E is very similar to that of the native enzyme with an overall average rmsd of 0.63 Å between the monomers. The positions of the active site amino acids were not significantly different with an average rmsd of only 0.15 Å. The crystal structure of NrfA Q263E revealed that Glu 263 is coordinated to the calcium I ion by only one of its oxygen atoms and in

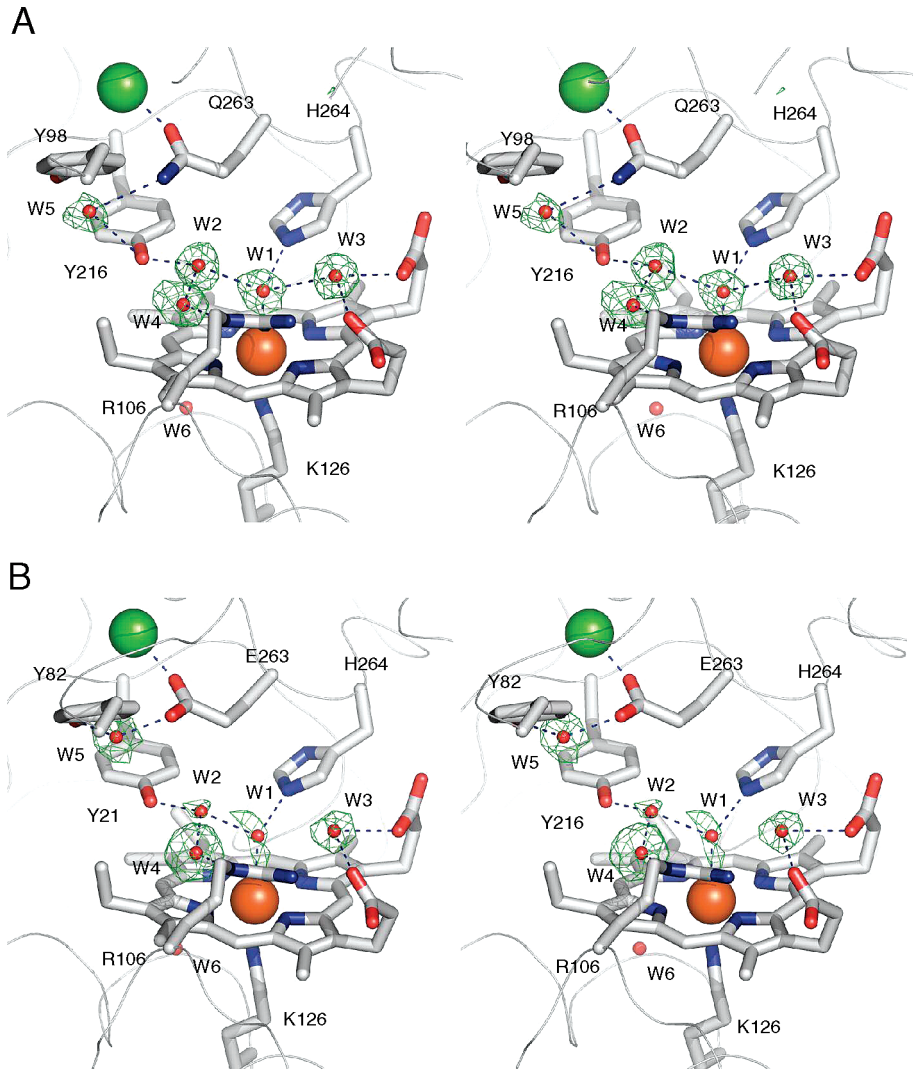

FIGURE 6: Stereoviews of the active sites of native and Q263 mutant NrfA enzymes. (A) Active site of native NrfA at 1.7 Å resolution. An $|F_o - F_c|$ omit map (calculated using experimentally determined structure factor amplitudes and with phases calculated for the final refined structure minus the active site water molecules) contoured at 5 σ is shown in green. The structure shown is the final experimentally determined structure with the five conserved active site residues and Tyr 82 shown in stick representation. The dashed lines indicate hydrogen bonds with distances less than 3.1 Å. The calcium I ion is shown as a green sphere. (B) Active site of NrfA Q263E refined at a resolution of 2.0 Å. An $|F_o - F_c|$ omit map calculated as for the native enzyme structure in (A) and contoured at 4 σ is shown in green. The dashed lines indicate hydrogen bonds between waters with distances less than 3.1 Å.

a similar conformation to Gln 263, rather than acting as a bidentate ligand as typically occurs between a carboxyl group and a calcium ion (Figure 6B). However, by comparing omit maps calculated in the region of the active site for native NrfA and NrfA Q263E structures (Figures 6A and B), it is evident that the networks of hydrogen bonded water molecules in the active sites of native NrfA and NrfA Q263E differ. The electron density corresponding to the water molecule that is hydrogen bonded to Tyr 216 in the native structure (W5) is diminished and appears to have been elongated. It has also shifted in position so that the hydrogen bond to Tyr 216 is lost and instead bridges Glu 263 and Tyr 82, thus breaking the extended hydrogen bond network involving the distal water molecule. The remaining conserved water molecules, including W2 and W3, are retained but show a similar diminution in their electron density levels. In the refined structure, the length of the bond between the distal water (W1) and the heme iron has increased to 2.58 ± 0.06 Å (Table 2). This increase in the heme−water ligand distance mirrors an increase in the B-factor of the distal water molecule; the active site water in the native enzyme structure has an average B-factor of 13.2 ± 1 Å^2, while in NrfA Q263E, it rises to 31.6 ± 2 Å^2. Similar increases in atomic temperature factors are observed for other conserved active site water molecules (W2−W3) forming the hydrogen bonded network at the active center (Figure 6 and Table 3). That it is only this complex of hydrogen bonded water molecules that is affected by the mutation is evidenced by the fact that the average B-factor calculated for all water molecules is almost unchanged following the mutation. In addition, the B-factors of other conserved active site water molecules remain similar. For example, W6, the water molecule buried in a pocket on the proximal side of heme 1 and adjacent to Lys 126 has a B-factor of 10.4 ± 1 Å^2 in the native structure and 13.8 ± 2 Å^2 in NrfA Q263E. The atomic temperature factors of Lys 126, the proximal ligand to the heme, also remains relatively unchanged (Table 2), consistent with the suggestion that the reason for the delocalization of the water molecules at the active site is caused by changes near the distal side of the heme.

Table 3: Temperature Factors (B-Factors) of Active Site Water Molecules in the Crystal Structures of Native NrfA and NrfA Q263E[a]

water molecule	native NrfA (Å^2)	NrfA Q263E (Å^2)
W1	13.2 ± 0.6	31.6 ± 1.7
W2	21.2 ± 0.2	34.8 ± 1.7
W3	12.1 ± 0.9	17.1 ± 0.9
W4	21.3 ± 1.2	18.9 ± 2.9
W5	36.5 ± 3.3	30.3 ± 2.2
W6	10.4 ± 0.7	13.8 ± 2.0
average B-factor for all waters in structure	31.4	31.6

[a] The values for the active site waters W1 to W6 are given ± standard error.

Both native NrfA and NrfA Q263E were crystallized under identical conditions at pH 7.5 but were shown to have different space groups. We do not consider the differences at the active site to be an artifact of either resolution or change in space group as the previously published *E. coli* NrfA structure, refined at the much lower resolution of 2.5 Å, was revealed to have a water molecule coordinated to the active site at a similar distance to the present high resolution structure of the native enzyme, despite being solved in a different space group. In addition, other water molecules in the active site were conserved and had correspondingly low temperature factors.

Disappointingly, our attempts to determine crystal structures for the nitrite adducts of both the native and mutant enzymes failed to deliver interpretable electron density for the bound ligand (data not shown). We presume this was due to the relatively weak binding of nitrite to both forms of the oxidized enzyme at the pH at which the crystals were grown and the X-ray data collection experiments were performed (pH 7.5). We note that the structure of the nitrite adduct of the *W. succinogenes* enzyme was determined from a crystal buffered at pH 5.7 (*12*).

DISCUSSION

The means by which enzymes tune their activities to the availability of their substrates is a question of continuing interest. This is of particular relevance for enzymes operating on simple substrates such as nitrite where the extended interaction surfaces available for binding offered by larger substrates are absent. In the case of *E. coli* cytochrome *c* nitrite reductase, the low micromolar K_m for nitrite confers on the enzyme the capacity to respire nitrite effectively in the physiological concentration range found in the gut (*33*). This work has illustrated the importance of a conserved active site glutamine residue 11 Å distant from the site of catalysis, which appears to offer no direct interaction with substrate or product in defining this affinity.

Comparison of both native NrfA and NrfA Q263E using EPR and MCD spectroscopies indicated that the active sites of both native enzymes were similar, with a water/hydroxide molecule retained as a ligand to the active site heme iron in both. A comparison of the enzymes using high resolution X-ray crystallographic data revealed that their structures were almost identical and that there were no significant changes in the positions of active site residues. However, examination of the refined positions and temperature factors of water molecules showed that mutation of glutamine 263 to glutamate ultimately breaks a highly coordinated arrangement of hydrogen bonded water molecules at the active site. These active site water molecules have increased temperature factors and therefore likely correspondingly lower occupancies (*34*). Any role they may play in stabilizing bound substrates may then have been compromised.

Surprisingly, in the crystal structure of *D. vulgaris* NrfA complexed with NrfH (*5*), the active site water has an average bond length of 2.80 ± 0.1 Å, much higher than the bond length observed in other published NrfA structures; the reasons for this are unclear, but heme Fe−water coordination distances of 2.7 Å have been identified in horseradish peroxidase crystal structures where the water forms a ligand to a hexa-coordinate high spin heme (*35*). While we cannot readily reason why the *D. vulgaris* NrfA active site water network is so different from that seen in other NrfA structures, our results show that a NrfA active site with disordered waters can reduce nitrite but will have a decreased affinity for nitrite. While *D. vulgaris* NrfA has been shown to reduce nitrite, no K_m has been published. However, the *D. vulgaris* NrfA enzyme has been shown to be constitutively expressed in the absence of nitrite and to reduce sulfite (*36*), thus the active site of this NrfA may not be optimized for nitrite.

In contrast to these subtle changes in the structure of the active site, the kinetic properties of NrfA were dramatically altered through this mutation. Although the V_{max} of nitrite reduction does not change significantly, the K_m increases by more than 10-fold. That similar K_m values arose in methyl viologen assays and protein film voltammetry indicates that the increased K_m of the mutant enzyme is independent of the nature of the electron donor and most likely associated with changes induced at the active site. Thus, these results provide compelling evidence that Gln 263 does not contribute significantly to the catalytic turnover of nitrite to ammonia. Instead the glutamine appears to play an important role in increasing the affinity of NrfA for nitrite at the active site of the enzyme. Certainly the choice of glutamine over the more usual glutamate for ligation of the essential calcium ion will result in a less-negatively charged substrate access channel that should promote binding of the negatively charged substrate, nitrite, in the active site.

Protein film voltammetry reveals that the Q263E mutation has a further consequence on NrfA activity in that more negative potentials are required to activate nitrite reduction. We have previously proposed that E_{cat} reflects in some part the reduction potential of the active site lysine-coordinated heme (*19*). The finding of a lower E_{cat} for NrfA Q263E than native enzyme suggests that the reduction potential of the lysine-coordinated heme is lower in the Q263E variant consistent with the introduction of additional negative charge into the active site. The lower potentials required to drive catalysis by NrfA Q263E may explain why this enzyme does not display an obvious boost in activity at maximum turnover rates despite a V_{max} predicted to be equal to that of native NrfA from the results of the methyl viologen assays. We note that absolute catalytic rates are not available from the PFV since the amount of electrocatalytically active enzyme is not known. The redox potential of methyl viologen has been measured as −450 mV, significantly lower than the catalytic potential of both native NrfA and NrfA Q263E, and therefore, in methyl viologen assays, no difference is

observed between the maximum activities of the native or Q263E forms of NrfA.

E_{switch} is slightly lower in NrfA Q263E than the native enzyme. We previously suggested that when an attenuation of activity is observed on accessing lower potentials, this is driven by reduction of one (or both) of the bis-histidine coordinated hemes lying near the dimer interface (*19*). When E_{switch} is sufficiently separated from E_{cat}, each potential may be correlated with the reduction potentials of the centers that modulate enzyme activity. However, for peaked catalytic wave shapes, E_{switch} and E_{cat} will to some extent reflect the consequences of overlapping the contributions from each process. As a result, the potential at the foot of the attenuation process, that is, where catalysis achieves a constant value at lower potentials, is likely to be a clearer reflection of the redox properties of the center responsible for the reductive attenuation than E_{switch} itself (Figures 5A and B). For NrfA Q263E, the foot of the attenuation occurs at potentials similar to that of native NrfA. Thus, we consider that the Q263E mutation has little effect on the properties of the center that when reduced, attenuates activity.

Despite being highly conserved among cytochrome *c* nitrite reductases, the calcium I ion of NrfA is too far from the catalytic site to play a direct part in the reaction cycle. However, the simple mutation of this glutamine residue to a glutamate introduces a hydrogen bond acceptor group in place of a donor in its side chain and removes an essential stabilizing component of a highly ordered network of hydrogen bonded water molecules in the active site. The mutation has significant additional effects, causing the heme−ligand bond to lengthen and the catalytic potential of the heme to decrease, and decreasing the affinity of the active site for nitrite while still maintaining hexa-coordination of the high-spin catalytic heme. Residue 263 lies at the boundary between the disordered waters of the solvent access channel and the highly ordered waters of the active site. Perturbation of this boundary causes a subset of the latter to increase in disorder and attenuate the affinity of the active site for the distal ligand.

REFERENCES

1. Richardson, D. J. (2000) Bacterial respiration: a flexible process for a changing environment. *Microbiology 146*, 551–571.
2. Simon, J. (2002) Enzymology and bioenergetics of respiratory nitrite ammonification. *FEMS Microbiol. Rev. 26*, 285–309.
3. Poock, S. R., Leach, E. R., Moir, J. W., Cole, J. A., and Richardson, D. J. (2002) Respiratory detoxification of nitric oxide by the cytochrome c nitrite reductase of Escherichia coli. *J. Biol. Chem. 277*, 23664–23669.
4. Hussain, H., Grove, J., Griffiths, L., Busby, S., and Cole, J. (1994) A seven-gene operon essential for formate-dependent nitrite reduction to ammonia by enteric bacteria. *Microbiology 12*, 153–163.
5. Rodriques, M. L., Oliveira, T. F., Pereira, I. A. C., and Archer, M. (2006) X-ray structure of the membrane-bound cytochrome c quinol dehydrogenase NrfH reveals novel heme coordination. *EMBO J. 25*, 5951–5960.
6. Clarke, T. A., Dennison, V., Seward, H., Burlat, B., Cole, J. A., Hemmings, A. M., and Richardson, D. J. (2004) Purification and spectropotentiometric characterization of *Escherichia coli* NrfB, a decaheme homodimer that transfers electrons to the decaheme periplasmic nitrite reductase complex. *J. Biol. Chem. 279*, 41333–41339.
7. Clarke, T. A., Cole, J. A., Richardson, D. J., and Hemmings, A. M. (2007) The crystal structure of the pentahaem c-type cytochrome NrfB and characterization of its solution-state interaction with the pentahaem nitrite reductase NrfA. *Biochem. J. 406*, 19–30.
8. Bamford, V. A., Angove, H. C., Seward, H. E., Thomson, A. J., Cole, J. A., Butt, J. N., Hemmings, A. M., and Richardson, D. J. (2002) Structure and spectroscopy of the periplasmic cytochrome c nitrite reductase from *Escherichia coli*. *Biochemistry 41*, 2921–2931.
9. Einsle, O., Stach, P., Messerschmidt, A., Simon, J., Kroger, A., Huber, R., and Kroneck, P. M. (2000) Cytochrome c nitrite reductase from *Wolinella succinogenes*. Structure at 1.6 Å resolution, inhibitor binding, and heme-packing motifs. *J. Biol. Chem. 275*, 39608–39616.
10. Einsle, O., Messerschmidt, A., Stach, P., Bourenkov, G. P., Bartunik, H. D., Huber, R., and Kroneck, P. M. (1999) Structure of cytochrome c nitrite reductase. *Nature 400*, 476–480.
11. Cuhna, C. A., Macieira, S., Dias, J. M., Almeida, G., Goncalves, L. L., Costa, C., Lampreia, J., Huber, R., Moura, J. J. G., Moura, I., and Romao, M. J. (2003) Cytochrome c nitrite reductase from *Desulfovibrio desulfuricans* ATCC 27774. The relevance of the two calcium sites in the structure of the catalytic subunit (NrfA). *J. Biol. Chem. 278*, 17455–17465.
12. Einsle, O., Messerschmidt, A., Huber, R., Kroneck, P. M. H., and Nesse, F. (2002) Mechanism of the six-electron reduction of nitrite to ammonia by cytochrome c nitrite reductase. *J. Am. Chem. Soc. 124*, 11737–11745.
13. Howes, B. D., Feis, A., Raimondi, L., Indiani, C., and Smulevich, G. (2001) The critical role of the proximal calcium ion in the structural properties of horseradish peroxidase. *J. Biol. Chem. 276*, 40704–40711.
14. Grove, J., Busby, S., and Cole, J. (1996) The role of the genes nrfEFG and ccmFH in cytochrome c biosynthesis in *Escherichia coli*. *Mol. Gen. Genet. 28*, 332–341.
15. Arslan, E., Schulz, H., Zufferey, R., Kunzler, P., and Thöny-Meyer, L. (1998) Overproduction of the *Bradyrhizobium japonicum* c-type cytochrome subunits of the cbb3 oxidase in *Escherichia coli*. *Biochem. Biophys. Res. Commun. 251*, 744–747.
16. Clarke, T. A., Mills, P. C., Poock, S. R., Butt, J. N., Cheesman, M. R., Cole, Hinton, J. C. D., Hemmings, A. M., Kemp, G., Söderberg, C., Spiro, S., Van Wonderen, J., and Richardson, D. J. (2007) *Escherichia coli* cytochrome c-nitrite reductase NrfA. *Methods Enzymol. 237*, 61–75.
17. Bergmeyer, H. U. and Beutler, H.-O. (1985) Methods of Enzymatic Analysis (Bergmeyer, H. U., ed.) 3rd ed., vol. VIII, pp. 454–461, Verlag Chemie, Weinheim, Deerfield Beach/ Florida, Basel.
18. Anderson, L. J., Richardson, D. J., and Butt, J. N. (2001) Catalytic protein film voltammetry from a respiratory nitrate reductase provides evidence for complex electrochemical modulation of enzyme activity. *Biochemistry 40*, 11294–307.
19. Angove, H. C., Cole, J. A., Richardson, D. J., and Butt, J. N. (2002) Protein film voltammetry reveals distinctive fingerprints of nitrite and hydroxylamine reduction by a cytochrome C nitrite reductase. *J. Biol. Chem. 277*, 23374–23381.
20. Leslie, A. G. (1999) Integration of macromolecular diffraction data. *Acta Crystallogr., Sect. D 55*, 1696–1702.
21. Evans, P. (2006) Scaling and assessment of data quality. *Acta Crystallogr., Sect. D 62*, 72–82.
22. Collaborative Computational Project, Number 4. (1994) The CCP4 Suite: programs for protein crystallography. *Acta Crystallogr., Sect. D 50*, 760–763.
23. Emsley, P., and Cowtan, K. (2004) Coot: model-building tools for molecular graphics. *Acta Crystallogr., Sect. D 60*, 2126–2132.
24. Murshudov, G. N., Vagin, A. A., and Dodson, E. J. (1997) Refinement of macromolecular structures by the maximum-likelihood method. *Acta Crystallogr. D 53*, 240–255.
25. Cohen, S. X., Morris, R. J., Fernandez, F. J., Jelloul, M. B., Kakaris, M., Parthasarathy, V., Lamzin, V. S., Kleywegt, G. J., and Perrakis, A. (2004) Towards complete validated models in the next generation of ARP/ wARP. *Acta Crystallogr., Sect. D 60*, 2222–2229.
26. Laskowski, R. A., MacArthur, M. W., Moss, D. S., and Thornton, J. M. (1993) PROCHECK: a program to check the stereochemical quality of protein structures. *J. Appl. Crystallogr. 26*, 283–291.
27. Cheesman, M. R., Greenwood, C., and Thomson, A. J. (1991) Magnetic circular-dichroism of hemoproteins. *Adv. Inorg. Chem. 36*, 201–255.
28. Gadsby, P. M. A., and Thomson, A. J. (1990) Assignment of the axial ligands of ferric ion in low-spin hemoproteins by near-infrared magnetic circular-dichroism and electron-paramagnetic resonance spectroscopy. *J. Am. Chem. Soc. 112*, 5003–5011.
29. Thomson, A. J., and Gadsby, P. M. A. (1990) A theoretical model of the intensity of the near-infrared porphyrin-to-iron charge-transfer transitions in low-spin iron(III) hemoproteins - a correlation

between the intensity of the magnetic circular-dichroism bands and the rhombic distortion parameter of iron. *J. Chem. Soc., Dalton Trans.* 1921–1928.
30. Cheesman, M. R., Oganesyan, V. S., Watmough, N. J., Butler, C. S., and Thomson, A. J. (2004) The nature of the exchange coupling between high-spin Fe(III) heme o3 and CuB(II) in *Escherichia coli* quinol oxidase, cytochrome bo3: MCD and EPR studies. *J. Am. Chem. Soc. 126*, 4157–4166.
31. Kajie, S., and Anraku, Y. (1986) Purification of a hexaheme cytochrome C552 from *Escherichia coli* K-12 and its properties as a nitrite reductase. *Eur. J. Biochem. 154*, 457–463.
32. Gwyer, J. D., Angove, H. C., Richardson, D. J., and Butt, J. N. (2004) Redox-triggered events in cytochrome c nitrite reductase. *Bioelectrochemistry 63*, 43–47.
33. Potter, L., Angove, H., Richardson, D. J., and Cole, J. A. (2001) Nitrate reduction in the periplasm of Gram negative bacteria. *Adv. Microbial Physiol. 45*, 52–102.
34. Carugo, O. (1999) Correlation between occupancy and B factor of water molecules in protein crystal structures. *Protein Eng. 12*, 1021–1024.
35. Smulevich, G., Feis, A., Indiani, C., Beccuci, M., and Marzocchi, M. P. (1999) Peroxidase-benzhydroxamic acid complexes: spectroscopic evidence that a Fe-H2O distance of 2.6 A can correspond to hexa-coordinate high-spin heme. *J. Biol. Inorg. Chem. 4*, 39–47.
36. Pereira, I. A., LeGall, J., Xavier, A. V., and Teixeira, M. (2000) Characterization of a heme c nitrite reductase from a non-ammonifying microorganism, *Desulfovibrio vulgaris* Hildenborough. *Biochim. Biophys. Acta 1481*, 119–130.
37. Krissinel, E., and Henrick, K. (2007) Inference of macromolecular assemblies from crystalline state. *J. Mol. Biol. 372*, 774–797.

BI702175W